Universität Stuttgart

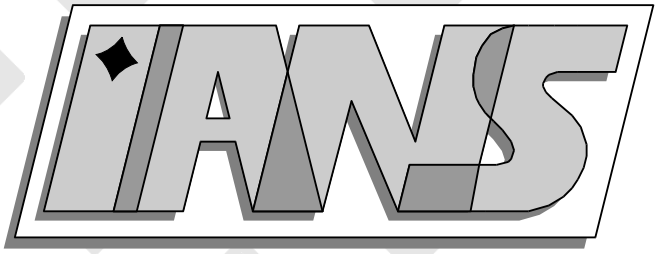

A comparison of mortar and Nitsche techniques for linear elasticity

Achim Fritz, Stefan Hüeber, Barbara I. Wohlmuth

Berichte aus dem Institut für Angewandte Analysis und Numerische Simulation

Preprint 2003/008

Universität Stuttgart

A comparison of mortar and Nitsche techniques for linear elasticity

Achim Fritz, Stefan Hüeber, Barbara I. Wohlmuth

Berichte aus dem Institut für Angewandte Analysis und Numerische Simulation

Preprint 2003/008

Institut für Angewandte Analysis und Numerische Simulation (IANS)
Fakultät Mathematik und Physik
Fachbereich Mathematik
Pfaffenwaldring 57
D-70 569 Stuttgart

E-Mail: ians-preprints@mathematik.uni-stuttgart.de
WWW: http://preprints.ians.uni-stuttgart.de

ISSN **1611-4176**

A COMPARISON OF MORTAR AND NITSCHE TECHNIQUES FOR LINEAR ELASTICITY

A. FRITZ*, S. HÜEBER*, B.I. WOHLMUTH*

Abstract. Domain decomposition techniques provide a powerful tool for the numerical approximation of partial differential equations. In this paper, we analyze the Nitsche method for the Lamé operator, establish a priori error estimates and compare this method with the mortar method using dual Lagrange multiplier spaces. Both methods can be applied to non matching triangulations. We use a multigrid algorithm to solve the algebraic systems. Although we have a mesh dependent bilinear form, optimal $\mathcal{W}$-cycle convergence rates can be obtained. Numerical results for the two methods with linear and quadratic finite elements illustrate the performance and flexibility of these non conforming discretization techniques.

Key words. mortar finite elements, Nitsche methods, domain decomposition, non matching triangulations, multigrid methods, mesh dependent bilinear form, linear elasticity

AMS subject classifications. 65N15, 65N30, 65N55

1. Introduction. For the efficient numerical approximation of boundary value problems, domain decomposition methods are often used and provide powerful techniques. In particular, non conforming techniques provide a more flexible approach. Here, we consider two non overlapping domain decomposition techniques and non matching triangulations at the inner boundaries of the subdomains. Non matching triangulations can arise, e.g., if the meshes on the different subdomains are generated independently from each other, or if one subdomain is sliding and no remeshing strategy is used. To use highly different mesh sizes on the different subdomains is of special interest in the case of corner singularities or in the case of different material parameters. Then in general, no strong continuity condition at the inner boundaries can be imposed on the discrete solution. There are several different approaches to deal with this situation. Here, we focus on mortar [Ben99, BMP93, BMP94] and Nitsche [Nit71, BH99, HP00, BHS01, HN01] techniques. In the case of mortar methods, the strong pointwise continuity condition is replaced by a weaker integral condition. There are several different but equivalent variational formulations. One possibility is to introduce the flux on the skeleton as additional unknown and to write the discrete variational formulation as a saddle point problem. To obtain a stable and optimal scheme, the discrete Lagrange multiplier space has to satisfy a uniform inf-sup condition and suitable approximation properties. Elimination of the Lagrange multiplier yields a positive definite formulation on the constrained mortar space. In the case of dual Lagrange multiplier spaces [Woh01], the elimination can be carried out locally. On the other hand, Nitsche techniques yield a symmetric and positive definite bilinear form on the unconstrained product space depending of the actual mesh size. To obtain a stable scheme, the jump of the solution has to be penalized. The mesh dependent bilinear form depends on a fixed parameter which has to be chosen large enough. In both situations, the resulting linear system can be efficiently solved in terms of multigrid methods.

Here, we present a comparison between the Nitsche and the mortar method for the Lamé equation in linear elasticity. We compare the theoretical results on the discretization errors and provide several numerical examples using linear and quadratic finite element spaces. In particular, we reformulate the mortar method and interpretate it as a Nitsche variant based on inexact integrals. We briefly recall the mortar method and its theoretical stability and convergence results in Section 2.1. The Nitsche method and the a priori estimates for the discretization errors are considered in Section 2.2. In Section 3, we apply a standard multigrid method on the Nitsche method. Optimal convergence rates can be established for the $\mathcal{W}$-cycle but not for the $\mathcal{V}$-cycle. Finally in Section 4, numerical results illustrating the performance and flexibility of these non confirming discretization techniques are given. We focus on the comparison of the L^2-error, the H^1-error and the errors on the skeleton for both methods. Additionally, we consider the influence

*Institute of Applied Analysis and Numerical Simulations (IANS), University of Stuttgart, Germany, {hueeber,wohlmuth}@ians.uni-stuttgart.de. This work was supported in part by the Deutsche Forschungsgemeinschaft, SFB 404, C12.

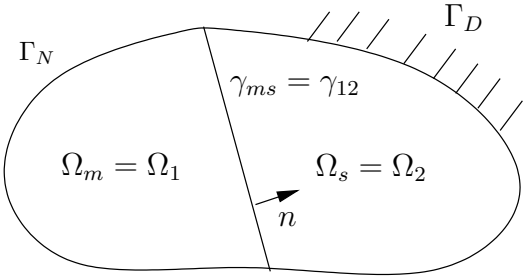

FIG. 2.1. *Decomposed domain* $\overline{\Omega} = \overline{\Omega}_1 \cup \overline{\Omega}_2$

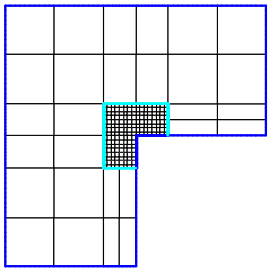

FIG. 2.2. *Non matching triangulations on* Ω

of the stabilization parameter on the discretization errors in case of the Nitsche method. In a last test series, we give the asymptotic convergence rates for the $\mathcal{W}$-cycle. As predicted by the theory, level independent multigrid convergence rates can be observed.

2. Non conforming discretizations based on domain decomposition. In this section, we will consider for a given bounded polygonal domain $\Omega \subset \mathbb{R}^2$ the boundary value problem for the displacement field $u \in \mathbb{R}^2$ for the equations of linear elasticity

$$\begin{aligned} -\operatorname{div} \boldsymbol{\sigma}(u) &= f, && \text{in} && \Omega, \\ u &= 0, && \text{on} && \Gamma_D, \\ \boldsymbol{\sigma}(u)\, n &= 0, && \text{on} && \Gamma_N, \end{aligned} \tag{2.1}$$

where the boundary $\Gamma = \partial\Omega$ is divided into two disjoint parts Γ_D and Γ_N with given displacements u on Γ_D and given stresses $\boldsymbol{\sigma}(u)\, n$ on Γ_N. By n we denote the outer unit normal vector of $\partial\Omega$, and we assume that Γ_D has a non zero measure. Let $\boldsymbol{\varepsilon}$ be the linearized strain tensor

$$\boldsymbol{\varepsilon}(u) = \frac{1}{2}\Big(\nabla u + (\nabla u)^\top\Big),$$

then the stress strain relation for a linear elastic material is given by Hooke's law

$$\boldsymbol{\sigma}_{ij} = \mathbf{C}_{ijkl}\boldsymbol{\varepsilon}_{kl}, \tag{2.2}$$

where the components of the symmetric and positive definite tensor $\mathbf{C}$ are

$$\mathbf{C}_{ijkl} = \lambda\, \delta_{ik}\delta_{kl} + \mu\, (\delta_{ik}\delta_{jl} + \delta_{il}\delta_{jk})$$

with the Lamé parameters λ and μ. Another possibility is to rewrite Hooke's law (2.2) as

$$\boldsymbol{\sigma} = \lambda \operatorname{tr}(\boldsymbol{\varepsilon}) + 2\mu\boldsymbol{\varepsilon}.$$

The domain Ω is decomposed into K non overlapping polygonal subdomains $\overline{\Omega} = \bigcup_{k=1}^{K} \overline{\Omega}_k$ with $\Omega_k \cap \Omega_l = \emptyset$ for $k \neq l$. We restrict ourselves to the geometrical conforming situation, where the intersection between the boundary of any two different subdomains $\partial\Omega_k \cap \partial\Omega_l$ for $k \neq l$ is either empty, a vertex, or a common edge. The skeleton γ is defined by

$$\gamma := \bigcup_{k,l=1}^{K} \gamma_{kl} \qquad \text{with the interfaces} \qquad \gamma_{kl} := \partial\Omega_k \cap \partial\Omega_l.$$

The normal vector n_{kl} on γ points from Ω_k to Ω_l. We restrict ourselves to the case of two subdomains. However, both methods can easily be generalized to more than two subdomains. We refer to [Ben99, BMP93, BMP94, Woh01] for an introduction to mortar methods and to [Nit71, BH99, HP00, BHS01, HN01] for Nitsche techniques.

We call $\Omega_m := \Omega_1$ master side and $\Omega_s := \Omega_2$ slave side of the interface γ, as it is shown in Figure 2.1. The vector n is the outer unit vector on $\partial\Omega_m$. The given locally quasi-uniform

triangulations on the subdomains are denoted by $\mathcal{T}_{h,\Omega_k}$ for $k = 1, 2$, and the associated Hilbert spaces are given by

$$V^k := \left\{ v \in \left[H^1(\Omega_k) \right]^2 \,:\, v_{|\partial\Omega_k \cap \Gamma_D} = 0 \right\}, \qquad k = 1, 2.$$

The restriction of $\mathcal{T}_{h,\Omega_k}$ on the interface gives the triangulation on γ associated with the slave side if $k = 2$ and with the master side if $k = 1$. We denote the two one dimensional meshes on γ by $\mathcal{T}_{h,\gamma_1}$ and $\mathcal{T}_{h,\gamma_2}$. Each element $e \in \mathcal{T}_{h,\gamma_k}$ is a boundary edge of $\mathcal{T}_{h,\Omega_k}$. In general, the two one dimensional meshes on γ are non matching, as it is shown in Figure 2.2. We only assume that there is a positive constant c_1 such that

$$h_{e_s} \leq c_1 h_{e_m}, \qquad 0 < c_1 < \infty, \tag{2.3}$$

for all elements $e_s \in \mathcal{T}_{h,\gamma_2}$ and for all $e_m \in \mathcal{T}_{h,\gamma_1}$ such that $e_m \cap e_s \neq \emptyset$, where $h_e := |e|$ is the length of an edge e.

Let the product space V be defined by $V := V^1 \times V^2$. Multiplying Equation (2.1) with a function $v^k \in V^k$, integrating over Ω_k and applying the homogeneous boundary conditions give rise to a variational problem. Using the notation $v := v^1 + v^2 \in V$ and $u := u^1 + u^2 \in V$ where v^k, $u^k \in V^k$ are extended by zero to Ω, we find that the weak solution of (2.1) satisfies

$$a(u, v) - \int_\gamma \left(\boldsymbol{\sigma}\left(u^2\right) n \right) [v] \, ds = (f, v)_0, \qquad v \in V, \tag{2.4}$$

where the bilinear form $a(\cdot, \cdot)$ and the linear form $(f, \cdot)_0$ are defined by

$$a(u, v) := \sum_{k=1}^{2} \int_{\Omega_k} \boldsymbol{\sigma}\left(u^k\right) : \nabla v^k \, dx, \qquad (f, v)_0 := \sum_{k=1}^{2} \int_{\Omega_k} f v^k \, dx.$$

The jump $[\cdot]$ is given by $[v] := v^1 - v^2$ on the interface γ. It is easy to see that the bilinear form $a(\cdot, \cdot)$ is continuous on $V \times V$ with respect to the broken H^1-norm on Ω. If $\Gamma_D \cap \partial\Omega_k$ has a non zero measure, then there holds Korn's inequality, see, e.g., [DL88], on each subdomain Ω_k, and $a(\cdot, \cdot)$ is elliptic on $V \times V$. However in the more general case, this does not hold. We use conforming finite element spaces of order p_k, $p_k \in \{1, 2\}$, on the subdomain Ω_k. The finite element space associated with the triangulation $\mathcal{T}_{h,\Omega_k}$ is denoted by $S_{p_k}(\Omega_k, \mathcal{T}_{h,\Omega_k})$. Then we have the discrete product space

$$V_h := \left[S_{p_1}(\Omega_1, \mathcal{T}_{h,\Omega_1}) \right]^2 \times \left[S_{p_2}(\Omega_2, \mathcal{T}_{h,\Omega_2}) \right]^2 \cap V \subset V. \tag{2.5}$$

2.1. Mortar formulation. In this subsection, we briefly recall the mortar formulation. We use the saddle point approach introduced in [Ben99]. It is based on a suitable Lagrange multiplier space and a duality pairing. Using the duality pairing between essential and natural boundary conditions, we set

$$b(v, \lambda) := \int_\gamma \lambda [v] \, ds, \qquad v \in V$$

and consider the discrete saddle point formulation: find $(u_h, \lambda_h) \in V_h \times M_h$ such that

$$\begin{array}{lcll} a(u_h, v_h) + b(v_h, \lambda_h) & = & (f, v_h)_0, & v_h \in V_h, \\ b(u_h, \mu_h) & = & 0, & \mu_h \in M_h. \end{array} \tag{2.6}$$

Here, we decompose γ into straight segments γ^l, $l = 1, \ldots, N$, and use the product space $M_h := \prod_{l=1}^{N} \left[M_h(\gamma^l) \right]^2$, where $M_h(\gamma^l)$ is a suitable Lagrange multiplier space. It is defined on the mesh associated with the slave side. There are different possibilities to define $M_h(\gamma^l)$. Roughly speaking,

it is sufficient if $M_h(\gamma^l)$ satisfies an inf-sup condition, an approximation property and the mortar projection is well defined. A natural choice is a modified trace space, see, e.g., [BMP94, BM97, BD98]. Here, we work with the dual Lagrange multiplier space defined in [Woh00]. If M_h is well chosen, the saddle point problem (2.6) has a unique solution and optimal a priori error estimates can be established. Under the assumption that $u \in \left[H^s(\Omega)\right]^2$, $\frac{3}{2} < s \leq p+1$, $p = \min\{p_1, p_2\}$, we have

$$\|u - u_h\|_{1,\Omega} + \|\lambda - \lambda_h\|_{-\frac{1}{2},\gamma} \leq Ch^{s-1}\|u\|_{s,\Omega}, \tag{2.7}$$

and $\|\cdot\|_{1,\Omega}$ is the broken H^1-norm on Ω. The norm $\|\cdot\|_{-\frac{1}{2},\gamma}$ denotes the broken $H^{-\frac{1}{2}}$-norm on the skeleton γ given by

$$\|\lambda\|_{-\frac{1}{2},\gamma} := \left(\sum_{l=1}^{N} \|\lambda\|^2_{-\frac{1}{2},\gamma^l}\right)^{\frac{1}{2}}, \qquad \lambda \in \prod_{l=1}^{N} H^{-\frac{1}{2}}(\gamma^l). \tag{2.8}$$

To get this estimate the so called LBB-condition or inf-sup condition for the discrete spaces V_h and M_h

$$\inf_{\mu_h \in M_h} \sup_{v_h \in V_h} \frac{b(v_h, \mu_h)}{\|v_h\|_{1,\Omega}\|\mu_h\|_{-\frac{1}{2},\gamma}} \geq C$$

and the approximation property for the discrete spaces V_h and M_h play an important role, see, e.g., [BF91],

$$\inf_{v_h \in V_h} \|u - v_h\|_{1,\Omega} \leq Ch^{s-1}\|u\|_{s,\Omega},$$
$$\inf_{\mu_h \in M_h} \|\lambda - \mu_h\|_{-\frac{1}{2},\gamma} \leq Ch^{s-1}\|u\|_{s,\Omega}.$$

Furthermore, if we assume H^2-regularity for the dual problem, we find

$$\|u - u_h\|_{0,\Omega} \leq Ch^s\|u\|_{s,\Omega}.$$

This a priori estimate in the L^2-norm is a consequence of the Aubin–Nitsche trick and the a priori estimate in the H^1-norm. For details, we refer to [BMP94, BM97, BD98, Ben99, Vas01, Woh01]. We remark that the same convergence order is given if the error in the Lagrange multiplier is considered in a suitably weighted L^2-norm. Moreover if the error in the energy norm is equilibrated distributed, the order of the Lagrange multiplier error in the weighted L^2-norm increases by 1/2.

2.2. Nitsche formulation. In this section, we consider an alternative possibility to solve our problem, the so called Nitsche formulation. This method is considered in [BH99, BHS01, HN01, HP00]. To formulate the problem, no Lagrange multiplier space is required, and we obtain a positive definite system on the unconstrained product space V_h. To guarantee that the resulting system is positive definite, the bilinear form has to be modified, and a mesh dependent one has to be used.

The average $\{\cdot\}$ on the interface γ is given by

$$\{u\} := \frac{1}{2}\left(u^1 + u^2\right) \qquad \text{and} \qquad \{\boldsymbol{\sigma}(u)\, n\} := \frac{1}{2}\left(\boldsymbol{\sigma}\left(u^1\right) n + \boldsymbol{\sigma}\left(u^2\right) n\right).$$

Motivated by (2.4), we expand our bilinear form $a(\cdot,\cdot)$ to a symmetric and mesh dependent one, denoted by $a_h(\cdot,\cdot)$, on the product space $V \times V$. For the scalar case we refer to [BH99, BHS01]. Our bilinear form $a_h^N(\cdot,\cdot)$ on $V \times V$ defined by

$$\begin{aligned} a_h^N(u,v) := \sum_{k=1,2} \int_{\Omega_k} \boldsymbol{\sigma}\left(u^k\right) : \nabla v^k \, dx - \int_{\gamma} \{\boldsymbol{\sigma}(u)\, n\}\,[v] \, ds \\ - \int_{\gamma} \{\boldsymbol{\sigma}(v)\, n\}\,[u] \, ds + \frac{\lambda+\mu}{2} \sum_{e \in \mathcal{T}_{h,\gamma_2}} \frac{\theta}{h_e} \int_e [u][v] \, ds, \end{aligned} \tag{2.9}$$

with a positive constant θ. Now the discrete variational problem is defined by the mesh dependent bilinear form: find $u_h \in V_h$ such that

$$a_h^N(u_h, v_h) = (f, v_h)_0, \qquad v_h \in V_h. \tag{2.10}$$

It is easy to see that this formulation is consistent with (2.1), if the weak solution of (2.1) is in $\left[H^{\frac{3}{2}+\varepsilon}(\Omega)\right]^2$ with $\varepsilon > 0$. Then $[u] = 0$ and $\boldsymbol{\sigma}(u^1)n - \boldsymbol{\sigma}(u^2)n = 0$, and we have

$$a_h^N(u, v) = (f, v)_0, \qquad v \in V. \tag{2.11}$$

For the a priori analysis, we introduce the mesh dependent norm, see, e.g., [BH99],

$$\|v\|_h^2 := \sum_{k=1,2} \int_{\Omega_k} \boldsymbol{\sigma}(v^k) : \nabla v^k \, dx + \|[v]\|_{\frac{1}{2},h,\gamma_2}^2, \qquad v \in V,$$

where the discrete $H^{\frac{1}{2}}$-norm on the interface γ_k is given by

$$\|[v]\|_{\frac{1}{2},h,\gamma_k}^2 := \sum_{e \in \mathcal{T}_{h,\gamma_k}} \frac{1}{h_e} \|[v]\|_{0,e}^2, \qquad v \in V.$$

Moreover, the discrete $H^{-\frac{1}{2}}$-norm on the interface γ_k is defined as

$$\|\mu\|_{-\frac{1}{2},h,\gamma_k}^2 := \sum_{e \in \mathcal{T}_{h,\gamma_k}} h_e \|\mu\|_{0,e}^2, \qquad \mu \in L^2(\gamma).$$

To show the ellipticity of the bilinear form $a_h^N(\cdot,\cdot)$ on $V_h \times V_h$, we use the well-known inverse property

$$h_T \|\nabla v_h\|_{0,\partial T}^2 \le C_I \|\nabla v_h\|_{0,T}^2, \qquad v_h \in V_h, \tag{2.12}$$

where $T \in \mathcal{T}_{h,\Omega_k}$, $k = 1, 2$, and h_T is the diameter of the element T. Note that the constant C_I depends on the order p in (2.5) and the shape regularity of the triangulation. For linear elasticity, we can bound the L^2-norm of $\boldsymbol{\sigma}(v_h)$ restricted on ∂T by the L^2-norm of ∇v_h restricted on T

$$h_T \|\boldsymbol{\sigma}(v_h)\|_{0,\partial T}^2 \le 2(\lambda+\mu) C_I \int_T \boldsymbol{\sigma}(v_h) : \nabla v_h \, dx \le 4(\lambda+\mu)^2 C_I \|\nabla v_h\|_{0,T}^2. \tag{2.13}$$

Now, we can show the ellipticity of the bilinear form $a_h^N(\cdot,\cdot)$ on the discrete space $V_h \times V_h$.

LEMMA 2.1. *Under the assumption that*

$$\theta > \theta_0 := (1 + c_1) C_I,$$

the bilinear form $a_h^N(\cdot,\cdot)$ is uniformly elliptic on $V_h \times V_h$.

Proof. We follow an approach given in [BH99] for the Laplace operator. In terms of (2.9), we find

$$\begin{aligned} a_h^N(v_h, v_h) &= \sum_{k=1,2} \int_{\Omega_k} \boldsymbol{\sigma}(v_h^k) : \nabla v_h^k \, dx - 2 \int_\gamma \{\boldsymbol{\sigma}(v_h) n\} [v_h] \, ds \\ &\quad + \frac{\lambda+\mu}{2} \sum_{e \in \mathcal{T}_{h,\gamma_2}} \frac{\theta}{h_e} \|[v_h]\|_{0,e}^2 \\ &\ge \sum_{k=1,2} \left(\int_{\Omega_k} \boldsymbol{\sigma}(v_h^k) : \nabla v_h^k \, dx - \left| \int_\gamma \big(\boldsymbol{\sigma}(v_h^k) n\big) [v_h] \, ds \right| \right) \\ &\quad + \frac{\lambda+\mu}{2} \sum_{e \in \mathcal{T}_{h,\gamma_2}} \frac{\theta}{h_e} \|[v_h]\|_{0,e}^2. \end{aligned}$$

By means of (2.13), we obtain for $\varepsilon > 0$

$$\left| \int_\gamma \big(\boldsymbol{\sigma}(v_h^2)n\big)[v_h]\ ds \right| \le \sum_{e\in\mathcal{T}_{h,\gamma_2}} \left(\frac{h_e}{2\varepsilon}\|\boldsymbol{\sigma}(v_h^2)n\|_{0,e}^2 + \frac{\varepsilon}{2h_e}\|[v_h]\|_{0,e}^2 \right)$$
$$\le \frac{(\lambda+\mu)C_I}{\varepsilon} \int_{\Omega_2} \boldsymbol{\sigma}(v_h^2) : \nabla v_h^2\ dx + \sum_{e\in\mathcal{T}_{h,\gamma_2}} \frac{\varepsilon}{2h_e}\|[v_h]\|_{0,e}^2$$

and

$$\left| \int_\gamma \big(\boldsymbol{\sigma}(v_h^1)n\big)[v_h]\ ds \right| \le \sum_{e\in\mathcal{T}_{h,\gamma_1}} \left(\frac{h_e}{2\varepsilon}\|\boldsymbol{\sigma}(v_h^1)n\|_{0,e}^2 + \frac{\varepsilon}{2h_e}\|[v_h]\|_{0,e}^2 \right)$$
$$\le \frac{(\lambda+\mu)C_I}{\varepsilon} \int_{\Omega_1} \boldsymbol{\sigma}(v_h^1) : \nabla v_h^1\ dx + \sum_{e\in\mathcal{T}_{h,\gamma_1}} \frac{\varepsilon}{2h_e}\|[v_h]\|_{0,e}^2$$
$$\le \frac{(\lambda+\mu)C_I}{\varepsilon} \int_{\Omega_1} \boldsymbol{\sigma}(v_h^1) : \nabla v_h^1\ dx + c_1 \sum_{e\in\mathcal{T}_{h,\gamma_2}} \frac{\varepsilon}{2h_e}\|[v_h]\|_{0,e}^2,$$

where we have used (2.3) for the last estimate. Finally, we find a lower bound for $a_h^N(v_h, v_h)$

$$a_h^N(v_h, v_h) \ge \sum_{k=1,2} \left(1 - \frac{(\lambda+\mu)C_I}{\varepsilon} \right) \int_{\Omega_k} \boldsymbol{\sigma}(v_h^k) : \nabla v_h^k\ dx$$
$$+ \left(\frac{\lambda+\mu}{2}\theta - (1+c_1)\frac{\varepsilon}{2} \right) \sum_{e\in\mathcal{T}_{h,\gamma_2}} \frac{1}{h_e}\|[v_h]\|_{0,e}^2.$$

Taking $\theta > (1+c_1)C_I$, then the ellipticity of the mesh dependent bilinear form is guaranteed on the discrete product space $V_h \times V_h$. ∎

We note, that θ does not depend on the Lamé parameters. Using the same techniques, we can show that the bilinear form $a_h^N(\cdot,\cdot)$ is continuous on $V_h \times V_h$. We remark that $a_h^N(\cdot,\cdot)$ is not continuous on $V \times V$. This is due to the fact that we cannot bound the discrete $H^{-\frac{1}{2}}$-norm of $\boldsymbol{\sigma}(u)n$ on the interface in terms of the H^1-norm of u on Ω.

To show the approximation property, we remark that for each function $v^k \in \big[H^s(\Omega_k)\big]^2$ with $1 < s \le p+1$ and for each subdomain Ω_k, $k = 1, 2$, we have

$$\inf_{v_h^k \in V_h^k} \left(\|\nabla(v^k - v_h^k)\|_{0,\Omega_k}^2 + \sum_{e\in\mathcal{T}_{h,\gamma_k}} \frac{1}{h_e}\|v^k - v_h^k\|_{0,e}^2 \right) \le C h^{2(s-1)} |v^k|_{s,\Omega_k}^2,$$

see, e.g., [Tho97]. Using (2.3) and (2.13), we get for $v \in \big[H^s(\Omega_1)\big]^2 \times \big[H^s(\Omega_2)\big]^2$ with $1 < s \le p+1$ the approximation property

$$\inf_{v_h \in V_h} \|v - v_h\|_h \le C h^{s-1} \left(|v|_{s,\Omega_1} + |v|_{s,\Omega_2} \right). \tag{2.14}$$

Next we will show the following a priori bound for the discretization error.

THEOREM 2.2. *For $\theta > \theta_0$, the variational formulation (2.10) has a unique solution $u_h \in V_h$. Let $u \in \big[H^s(\Omega)\big]^2$ with $\frac{3}{2} < s \le p+1$ be the solution of (2.1), then we have the a priori error estimate*

$$\|u - u_h\|_h \le C h^{s-1} |u|_{s,\Omega}.$$

Furthermore, if H^2-regularity is assumed, we obtain the following a priori estimate in the L^2-norm

$$\|u - u_h\|_{0,\Omega} \le C h^s |u|_{s,\Omega}.$$

Proof. The fact that the variational formulation (2.10) has a unique solution is a direct consequence of the Lemma of Lax–Milgram and the ellipticity of the continuous mesh dependent bilinear form $a_h^N(\cdot,\cdot)$ on the space $V_h \times V_h$. Using $V_h \subset V$ and (2.11), the Galerkin orthogonality

$$a_h^N(u - u_h, v_h) = (f, v_h)_0, \qquad v_h \in V_h \tag{2.15}$$

holds, and we can use conforming techniques to establish a priori estimates. To prove the first a priori estimate, we follow an idea presented in [BH99] for the Laplace operator. We start with the triangle inequality

$$\|u - u_h\|_h \leq \|u - v_h\|_h + \|u_h - v_h\|_h, \qquad v_h \in V_h. \tag{2.16}$$

In terms of Lemma 2.1 and the Galerkin orthogonality (2.15), we can bound the second term by

$$\begin{aligned} C\|u_h - v_h\|_h^2 &\leq a_h^N(u_h - v_h, u_h - v_h) = a_h^N(u - v_h, u_h - v_h) \\ &= \sum_{k=1,2} \int_{\Omega_k} \boldsymbol{\sigma}(u - v_h) : \nabla(u_h - v_h)\, dx - \int_\gamma \{\boldsymbol{\sigma}(u - v_h)n\}\, [u_h - v_h]\, ds \\ &\quad - \int_\gamma \{\boldsymbol{\sigma}(u_h - v_h)n\}\, [u - v_h]\, ds + \sum_{e \in \mathcal{T}_{h,\gamma_2}} \frac{\theta}{h_e} \int_e [u - v_h][u_h - v_h]\, ds. \end{aligned}$$

We recall that the bilinear form $a_h^N(\cdot,\cdot)$ is not continuous on $V \times V$. Using the Cauchy–Schwarz inequality, the inverse properties (2.12) and (2.13), we obtain

$$\|u_h - v_h\|_h^2 \leq C\|u_h - v_h\|_h \left(\|u - v_h\|_h + \left(\sum_{e \in \mathcal{T}_{h,\gamma_2}} h_e \|\nabla(u - v_h)\|_{0,e}^2 \right)^{\frac{1}{2}} \right). \tag{2.17}$$

To bound the term $h_e^{\frac{1}{2}} \|\nabla(u - v_h)\|_{0,e}$, we use a Scott–Zhang type projection operator P_h and the Lagrange interpolation operator I_h. Using the inverse estimate (2.12) and the trace theorem, we get for $s > \frac{3}{2}$ with $w_h = P_h \nabla u$

$$\begin{aligned} h_e^{\frac{1}{2}} \|\nabla(u - I_h u)\|_{0,e} &\leq h_e^{\frac{1}{2}} \big(\|\nabla u - w_h\|_{0,e} + \|\nabla I_h u - w_h\|_{0,e} \big) \\ &\leq C\big(h_e^{s-1} |\nabla u|_{s-1,\omega_e} + \|u - I_h u\|_{1,T_e} + \|\nabla u - w_h\|_{0,T_e} \big) \\ &\leq C\big(h_e^{s-1} |u|_{s,\omega_e} + h_e^{s-1} |u|_{s,T_e} + h_e^{s-1} |\nabla u|_{s-1,\omega_e} \big) \\ &\leq C h_e^{s-1} |u|_{s,\omega_e}, \end{aligned} \tag{2.18}$$

where the subset ω_e of Ω consists of the element T_e, $e \subset \partial T_e$, and all elements of the triangulation $\mathcal{T}_{h,\Omega_2}$, which have either a common vertex or a common edge with the element T_e. Then, the shape regularity of the triangulation yields

$$\left(\sum_{e \in \mathcal{T}_{h,\Omega_2}} h_e \|\nabla(u - v_h)\|_{0,e}^2 \right)^{\frac{1}{2}} \leq C h^{s-1} |u|_{s,\Omega_2}.$$

Combining the approximation property (2.14) and (2.17), we obtain from (2.16) the a priori estimate for the discretization error $u - u_h$ in the mesh dependent norm. A standard Aubin–Nitsche argument gives the a priori estimate for the discretization error in the L^2-norm. Let $w \in \big[H_0^1(\Omega)\big]^2$ be the solution of the dual problem. Then, we find in terms of the Galerkin

orthogonality (2.15)

$$\begin{aligned}\|u-u_h\|_{0,\Omega}^2 &= a_h^N(w,u-u_h) = a_h^N(w-w_h,u-u_h)\\ &\le C\prod_{v=w,u}\left(\|v-v_h\|_h + \left(\sum_{e\in\mathcal{T}_{h,\gamma_2}} h_e\|\nabla(v-v_h)\|_{0,e}^2\right)^{\frac{1}{2}}\right)\\ &\le C\big(h|w|_{2,\Omega}\big)\big(h|u|_{2,\Omega}\big),\end{aligned}$$

where the first estimate is based on the same techniques as the proof of (2.17). For the last estimate, we follow the proof of (2.18) and use the approximation property (2.14) for the term in $w-w_h$ with $s=2$ and for the term in $u-u_h$ with $\frac{3}{2}<s\le p+1$. Now, the a priori estimate for the L^2-norm results from the H^2-regularity assumption. ∎

Additionally, we can obtain a priori estimates for the flux and the trace on the interface.

THEOREM 2.3. *For $\frac{3}{2}<s\le p+1$, we have for the L^2-norm of the jump of the discrete solution u_h on the interface the upper bound*

$$\|[u_h]\|_{0,\gamma} \le Ch^{s-\frac{1}{2}}|u|_{s,\Omega}.$$

For the error of the flux on the interface, we get the a priori error estimate

$$h^{\frac{1}{2}}\|\boldsymbol{\sigma}(u-u_h)n\|_{0,\gamma} \le Ch^{s-1}|u|_{s,\Omega}.$$

Furthermore, we obtain for the trace the a priori estimate

$$h^{-\frac{1}{2}}\|u-u_h\|_{0,\gamma} \le Ch^{s-1}|u|_{s,\Omega}.$$

Proof. We remark that the mesh dependent norm $\|\cdot\|_h$ measures the nonconformity of the discrete solution u_h. A direct consequence of Theorem 2.2 is

$$\|[u-u_h]\|_{0,\gamma} = \|[u_h]\|_{0,\gamma} \le Ch^{s-\frac{1}{2}}|u|_{s,\Omega}.$$

With $w_h = P_h\nabla u$, the inverse inequality (2.12), (2.13) and the trace theorem, we find

$$\begin{aligned}h^{\frac{1}{2}}\|\boldsymbol{\sigma}(u-u_h)n\|_{0,\gamma} &\le Ch^{\frac{1}{2}}\big(\|\nabla u-w_h\|_{0,\gamma}+\|\nabla u_h-w_h\|_{0,\gamma}\big)\\ &\le Ch^{s-1}|\nabla u|_{s-\frac{3}{2},\gamma} + C\big(|u-u_h|_{1,\Omega}+\|\nabla u-w_h\|_{0,\Omega}\big)\\ &\le Ch^{s-1}|\nabla u|_{s-1,\Omega} + C\big(h^{s-1}|u|_{s,\Omega}+h^{s-1}|\nabla u|_{s-1,\Omega}\big)\\ &\le Ch^{s-1}|u|_{s,\Omega}.\end{aligned}$$

Moreover, we obtain by using the same techniques as before an upper bound for the the trace of $u-u_h$

$$\begin{aligned}h^{-\frac{1}{2}}\|u-u_h\|_{0,\gamma} &\le Ch^{-\frac{1}{2}}\big(\|u-P_hu\|_{0,\gamma}+\|P_hu-u_h\|_{0,\gamma}\big)\\ &\le Ch^{s-1}|u|_{s,\Omega} + Ch^{-1}\big(\|u-u_h\|_{0,\Omega}+\|u-P_hu\|_{0,\Omega}\big)\\ &\le Ch^{s-1}|u|_{s,\Omega}.\end{aligned}$$

The same qualitative result can be obtained for the trace in the $H^{1/2}$-norm. ∎

REMARK 2.1. *Moreover, if the L^2- and the H^1-error are equilibrated distributed, the error in the weighted norm for the flux and the values on the interface are of order $h^{\frac{3}{2}}$, if we use linear elements, i.e., $p=1$, and if u is regular enough. Then we have the estimates*

$$\begin{aligned}h^{\frac{1}{2}}\|\boldsymbol{\sigma}(u-u_h)n\|_{0,\gamma} &\le Ch^{\frac{3}{2}}|u|_{2,\Omega},\\ h^{-\frac{1}{2}}\|u-u_h\|_{0,\gamma} &\le Ch^{\frac{3}{2}}|u|_{2,\Omega},\\ h^{-\frac{1}{2}}\|[u_h]\|_{0,\gamma} &\le Ch^{\frac{3}{2}}|u|_{2,\Omega}.\end{aligned} \tag{2.19}$$

REMARK 2.2. *We easily can expand our bilinear form (2.9) to one, which is symmetric with respect to the length h_e of the elements on the interface γ and to the Lamé parameters. The bilinear form (2.9) can be replaced by*

$$\begin{aligned} a_h^N(u_h, v_h) := & \sum_{k=1,2} \int_{\Omega_k} \boldsymbol{\sigma}\left(u_h^k\right) : \nabla v_h^k \, dx - \int_\gamma \{\boldsymbol{\sigma}(u_h)\, n\}\, [v_h] \, ds \\ & - \int_\gamma \{\boldsymbol{\sigma}(v_h)\, n\}\, [u_h] \, ds + \frac{\lambda_1 + \mu_1}{2} \sum_{e \in \mathcal{T}_{h,\gamma_1}} \frac{\theta}{h_e} \int_e [u_h][v_h] \, ds \\ & + \frac{\lambda_2 + \mu_2}{2} \sum_{e \in \mathcal{T}_{h,\gamma_2}} \frac{\theta}{h_e} \int_e [u_h][v_h] \, ds, \end{aligned}$$

where λ_k, μ_k are the Lamé parameters on the subdomain Ω_k. Using the modified mesh dependent norm

$$\|v\|_h^2 := \sum_{k=1,2} \int_{\Omega_k} \boldsymbol{\sigma}(v^k) : \nabla v^k \, dx + \|[v]\|^2_{\frac{1}{2},h,\gamma_1} + \|[v]\|^2_{\frac{1}{2},h,\gamma_2},$$

the stability and a priori error analysis does not require (2.3).

In the rest of this section, we compare the mortar with the Nitsche method. There are different possibilities to obtain the mortar finite element solution. It is well known that the saddle point problem (2.6) is equivalent to

$$a(u_h, v_h) = (f, v_h)_0, \quad v_h \in V_h^c,$$

where the constrained space V_h^c is given by $V_h^c := \{v_h \in V_h \, : \, b(v_h, \mu_h) = 0, \ \mu_h \in M_h\}$. To compare the Nitsche with the mortar method, we work with a third equivalent formulation. Using dual Lagrange multipliers, the mesh dependent operator Q_h defined by

$$Q_h v := \sum_{i=1}^{m_h} \frac{\int_\gamma [v_h] \ \psi_i \ ds}{\int_\gamma \phi_i \ ds} \phi_i \tag{2.20}$$

is a projection. Here $2m_h$ is the dimension of M_h, ψ_i are the dual basis functions of $\prod_{l=1}^N M_h(\gamma^l)$ and ϕ_i are the nodal basis functions on the slave side, see [Woh01] for details. We note that Q_h is not a projection if we replace the dual Lagrange multiplier space by the standard one. Static condensation of the Lagrange multiplier yields an equivalent positive definite variational formulation on the unconstrained product space V_h: find $u_h \in V_h$ such that

$$a_h^m(u_h, v_h) = (f, v_h - Q_h v_h)_0, \quad v_h \in V_h, \tag{2.21}$$

where $a_h^m(u_h, v_h) := a(u_h, v_h) - a(u_h, Q_h v_h) - a(Q_h u_h, v_h) + 2a(Q_h u_h, Q_h v_h)$, see [Woh01]. We remark that (2.21) defines a mesh dependent bilinear form on $V_h \times V_h$ as it is done in the Nitsche formulation. From now on, we denote the mortar solution (u_h, λ_h) by (u_h^m, λ_h^m) and the Nitsche solution u_h by u_h^N and the mesh dependent bilinear forms by $a_h^m(\cdot,\cdot)$ and $a_h^N(\cdot,\cdot)$, respectively. Now, we consider the difference between $a_h^m(\cdot,\cdot)$ and $a_h^N(\cdot,\cdot)$ in more detail. In both cases, the bilinear form applied to v_h, w_h is reduced to the standard one if the jump of v_h and w_h is zero. Both bilinear forms have four terms. The first one is the same. We recall that the Lagrange multiplier in the mortar formulation is an approximation of the flux $\boldsymbol{\sigma}(u)n$. Thus, we can interpret the Lagrange multiplier as an approximation of $\{\boldsymbol{\sigma}(u_h)n\}$. Using the observation that

$$b(Q_h v_h, \lambda_h^m) = (f, Q_h v_h)_0 - a(u_h^m, Q_h v_h) = b(v_h, \lambda_h^m) = \int_\gamma \lambda_h^m [v_h] \, ds,$$

we find that $(f, Q_h v_h)_0 - a(u_h^m, Q_h v_h)$ approximates

$$\int_\gamma \{\boldsymbol{\sigma}(u_h^m)n\}[v_h]\ ds.$$

Thus the second term in both bilinear forms approximates $\int_\gamma \{\boldsymbol{\sigma}(u)n\}[v_h]\ ds$. For both mesh dependent bilinear forms the third term $a(Q_h u_h^m, v_h)$ and $\int_\gamma \{\boldsymbol{\sigma}(v_h^N)n\}[u_h]\ ds$, respectively, is added due to symmetry reasons and is equal to zero if the finite element solution is exact. Finally the fourth term, given by $2a(Q_h u_h^m, Q_h v_h)$ in the mortar setting and by $\sum_{e\in\mathcal{T}_{h;\gamma_2}} \frac{\theta}{h_e}\int_e \{\boldsymbol{\sigma}(u_h^N)n\}[v_h]\ ds$ for the Nitsche approach, can be regarded as a penalty term which guarantees the stability of the approach and the optimal order of the consistency error. In both cases this term measures the nonconformity of the solution and is equal to zero if the finite element solution is exact. Using the variational problem (2.21) to obtain the mortar finite element solution, we find that mortar and Nitsche techniques are very close although the starting point is very different. The main difference is the use of the exact jump in case of the Nitsche method, whereas a weaker integral form of the jump is used in case of the mortar method. This can be interpretated as a special numerical quadrature formula. As a consequence, we obtain a discrete solution satisfying a weak continuity condition, i.e., $Q_h u_h^m = 0$. The main advantage of the Nitsche method compared to the mortar approach is that it does not depend on a Lagrange multiplier space. Mortar methods can be realized very efficiently if dual Lagrange multipliers are used. However, the construction of good dual Lagrange multipliers space in 3D for higher order finite elements is tricky. If we have a locally defined dual Lagrange multiplier space, the complexity of assembling $a_h^m(\cdot,\cdot)$ and $a_h^N(\cdot,\cdot)$ has the same order. On the other hand, the main advantage of the mortar method compared to the Nitsche approach is that it does not depend on a stabilization parameter. In the mortar setting, highly different mesh sizes, Lamé parameters and/or an inhomogeneous elasticity tensor enters directly in the stabilization term, whereas in the Nitsche method we have to fix the scalar stabilization parameter. The surface integrals in the Nitsche formulation are replaced by volume integrals on a strip of width h in the mortar case.

3. Multigrid Method. For an introduction to multigrid methods, we refer to [Hac85, Bra95]. In this section, we show that the symmetric $\mathcal{W}$-cycle multigrid algorithm for our mesh dependent bilinear form $a_h^N(\cdot,\cdot)$ of the Nitsche formulation yields level independent convergence rates. Let $\mathcal{T}_{h,\Omega}^l$ be the triangulation on level l with mesh size h_l defined by the maximal diameter of the elements. We get our triangulation $\mathcal{T}_{h,\Omega}^l$ on level l from a uniform refinement step from the triangulation $\mathcal{T}_{h,\Omega}^{l-1}$ on the coarser level $l-1$. Every element on level $l-1$ is divided into four subelements. Then there holds

$$\mathcal{T}_{h,\Omega}^l \subset \mathcal{T}_{h,\Omega}^{l-1}, \qquad h_l = \frac{1}{2}h_{l-1}, \qquad l = 1,\dots,L.$$

As a consequence, we have for the finite element spaces V_h^l the relation $V_h^{l-1} \subset V_h^l$, $l = 1,\dots,L$, and we can choose the prolongation operator $\mathcal{I}_{l-1}^l$ from level $l-1$ to level l as natural embedding operator. The algebraic representation of the restriction operator $\mathcal{I}_l^{l-1}$ from level l to level $l-1$ is set to be the transposed of the prolongation. Let $a_l(\cdot,\cdot)$ be the bilinear form $a_h^N(\cdot,\cdot)$ on level l. Having in mind (2.9), we obtain

$$a_l\left(\mathcal{I}_{l-1}^l v_{l-1}, \mathcal{I}_{l-1}^l v_{l-1}\right) \le 2a_{l-1}\left(v_{l-1}, v_{l-1}\right), \qquad v_{l-1} \in V_h^{l-1}. \tag{3.1}$$

Let the operator $P_{l-1} : V_h^l \to V_h^{l-1}$ be defined by

$$a_l\left(v_l, \mathcal{I}_{l-1}^l w_{l-1}\right) = a_{l-1}\left(P_{l-1}v_l, w_{l-1}\right), \qquad w_{l-1} \in V_h^{l-1},$$

and $A_l : V_h^l \to V_h^l$ denotes the symmetric positive definite operator satisfying

$$a_l\left(w_l, v_l\right) = \left(A_l w_l, v_l\right), \qquad w_l, v_l \in V_h^l,$$

where $(\cdot,\cdot)$ stands for the Euclidean inner product on the discrete spaces V_h^l with the Euclidean norm $\|v_l\|_2^2 = (v_l, v_l)$, $v_l \in V_h^l$. We use standard nodal basis functions and identify the function $v_l \in V_h^l$ with its vector representation in $\mathbb{R}^{n_l}$, where n_l denotes the dimension of the space V_h^l. We point out that the eigenvalues of the operators A_l are bounded by a positive constant C independent of l. Using the continuity of $a_l(\cdot,\cdot)$ on $V_h^l \times V_h^l$, an inverse inequality and the quasi-uniformity of the triangulation, we find

$$a_l(v_l, v_l) \leq C\|v_l\|_h^2 \leq C\left(\frac{1}{h_l^2}\|v_l\|_{0,\Omega}^2 + \frac{1}{h_l}\|[v_l]\|_{0,\gamma}^2\right) \leq C\|v_l\|_2^2. \tag{3.2}$$

Thus the penalty term in our bilinear form (2.9) does not change the qualitative bounds for the eigenvalues. As smoothing operator, we use a damped Richardson iteration with damping factor $\frac{1}{\varrho_l}$, where ϱ_l denotes the spectral radius of A_l. To get the a priori estimate, the following approximation property is required

$$\left|a_l\left(\left(Id - \mathcal{I}_{l-1}^l P_{l-1}\right)v_l, v_l\right)\right| \leq C\|A_l v_l\|_2^2, \qquad v_l \in V_h^l. \tag{3.3}$$

This follows from the assumed H^2-regularity of the problem and the a priori estimates in the L^2-norm for the discretization error. To give a relation of the error after one multigrid step, we define the error operator E_l on level l for the $\mathcal{W}$-cycle recursively by

$$E_0 := 0, \qquad E_l := R_l^m\left(Id - \mathcal{I}_{l-1}^l\left(Id - E_{l-1}^2\right)P_{l-1}\right)R_l^m, \qquad l > 0.$$

The so called relaxation operator R_l is defined by $R_l := Id - \frac{1}{\varrho_l}A_l$ and m denotes the number of pre- and post-smoothing steps. Furthermore to show level independent convergence rates, we need a smoothing property

$$\|A_l R_l^m v_l\|_2^2 \leq \frac{C}{2m}\Big(a_l\left(v_l, v_l\right) - a_l\left(R_l^m v_l, R_l^m v_l\right)\Big), \tag{3.4}$$

which holds with some positive constant C independent of the level l. This is a consequence of the property of the Richardson iteration and the upper bound for the eigenvalues of the operators A_l. Let $u_l \in V_h^l$ be the exact solution of the algebraic equation $A_l u_l = f_l$ on level l and $u_l^{i+1} \in V_h^l$ be the next iterate of one multigrid step on level l with the previous iterate $u_l^i \in V_h^l$, then there holds for the error

$$u_l - u_l^{i+1} = E_l\left(u_l - u_l^i\right), \qquad l \geq 0.$$

The error operator E_l is symmetric with respect to the bilinear form $a_l(\cdot,\cdot)$. Now the following convergence result holds.

THEOREM 3.1. *The $\mathcal{W}$-cycle with m pre- and post-smoothing steps yields level independent convergence rates. Moreover, we have for the error propagation operator*

$$a_l\left(E_l v_l, E_l v_l\right) \leq \gamma^2 a_l(v_l, v_l), \qquad v_l \in V_h^l$$

with

$$\gamma := \frac{C}{C + 2m} < 1,$$

where C is a positive constant independent of l.

Proof. The basic tools for the proof are the approximation property (3.3), the smoothing property (3.4), the stability of the prolongation (3.1) and the bound for the eigenvalues (3.2). For details, we refer to [Bra95]. ∎

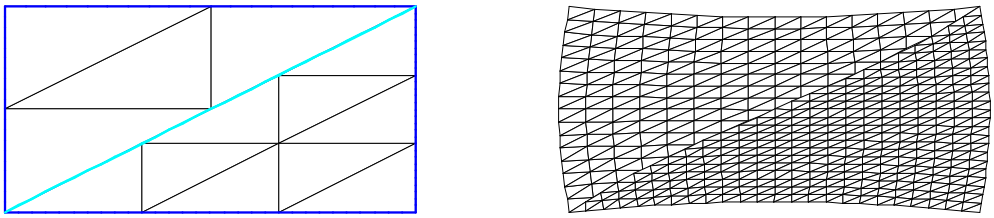

FIG. 4.1. *Initial triangulation and distorted grid*

4. Numerical results. In this section, we present some numerical examples for the non conforming domain decomposition methods discussed in the previous sections. Non matching initial triangulations and uniform refinement techniques are used. We provide numerical results for the Nitsche method and for the mortar method. In the case of the mortar method, we use a dual Lagrange multiplier, see, e.g., [Woh00]. To solve the arising algebraic equations, we use multigrid methods. A standard multigrid scheme is applied to the Nitsche formulation. For the mortar approach, we work with the positive definite formulation on the unconstrained product space and use the multigrid approach proposed in [WK01]. This multigrid scheme is based on the orthogonality of the jump of the mortar solution on the Lagrange multiplier space. Although the unconstrained product spaces are nested, a modified prolongation operator is defined. The modification can be carried out as a local postprocess of lower complexity. In all examples, we set the elasticity module to be $E = 200$ and the Poison number to be $\nu = 0.3$. Then the Lamé parameters are $\lambda = 115.38$ and $\mu = 76.92$. In the case of linear finite elements, we set $\frac{\lambda+\mu}{2}\theta = 500$, and in the case of quadratic finite elements we use $\frac{\lambda+\mu}{2}\theta = 1500$. This choice is motivated by the fact that in the quadratic case the constant C_I of the inverse inequality is greater. For simplicity of notation in the following the error in the H^1-error is in more precisely the error in the H^1-seminorm. The implementation is based on the finite element toolbox UG, see [BBJ+97].

4.1. Linear finite elements. In a first example, we consider two subdomains and use conforming piecewise linear elements on each subdomain. Let the domain $\Omega := (-1,\, 1) \times (-0.5,\, 0.5)$ be decomposed into two disjoint subdomains Ω_1 and Ω_2, defined by

$$\Omega_1 := \left\{(x_1, x_2)^\top \in \Omega \,:\, x_2 > 0.5x_1\right\} \quad \text{and} \quad \Omega_2 := \left\{(x_1, x_2)^\top \in \Omega \,:\, x_2 < 0.5x_1\right\}.$$

We set the master side to be Ω_1 and Ω_2 to be the slave side. For the solution $u(x) = (0.2x_1(0.25 - x_2^2),\, -0.1x_2(1-x_1^2))^\top$, we compute the corresponding volume force $f(x)$ and the Dirichlet boundary conditions. The volume force is then given by $(0.2\mu x_1 - 0.2\lambda x_1,\, 0.2\mu x_2 + 0.4\lambda x_2)^\top$. Figure 4.1 shows the initial non matching triangulation and the distorted grid after three uniform refinement steps.

TABLE 4.1
Relative $L^2(\Omega)$-, relative $H^1(\Omega)$-error of u_h, discrete $H^{\frac{1}{2}}(\gamma)$-error of the jump of u_h and the convergence orders for the Nitsche method for linear finite elements.

level	$\|u-u_h\|_{0,\Omega}$		$\|u-u_h\|_{1,\Omega}$		$\|[u_h]\|_{\frac{1}{2},h,\gamma}$	
0	$3.049091e-01$	–	$6.104212e-01$	–	$2.662975e-02$	–
1	$7.786115e-02$	1.96	$3.174141e-01$	0.94	$9.901271e-03$	1.42
2	$1.859063e-02$	2.06	$1.602452e-01$	0.98	$3.392599e-03$	1.54
3	$4.576805e-03$	2.02	$8.023026e-02$	0.99	$1.206764e-03$	1.49
4	$1.139600e-03$	2.00	$4.009512e-02$	1.00	$4.320825e-04$	1.48
5	$2.844351e-04$	2.00	$2.003559e-02$	1.00	$1.541486e-04$	1.48
6	$7.104255e-05$	2.00	$1.001384e-02$	1.00	$5.478419e-05$	1.49
theory		2.00		1.00		1.50

The discretization errors for the Nitsche method with linear finite elements, i.e., $p = 1$, are

TABLE 4.2
Discrete $H^{\frac{1}{2}}(\gamma)$-, discrete $H^{-\frac{1}{2}}(\gamma)$-error of u_h on the master and the slave side and the convergence orders for the Nitsche method for linear finite elements.

l	$\|u^1 - u_h^1\|_{\frac{1}{2},h,\gamma_1}$		$\|u^2 - u_h^2\|_{\frac{1}{2},h,\gamma_2}$		$\|(\boldsymbol{\sigma}^1 - \boldsymbol{\sigma}_h^1)n\|_{-\frac{1}{2},h,\gamma_1}$		$\|(\boldsymbol{\sigma}^2 - \boldsymbol{\sigma}_h^2)n\|_{-\frac{1}{2},h,\gamma_2}$	
0	$2.8426e-02$	–	$2.3155e-02$	–	$3.2754e+01$	–	$2.0765e+01$	–
1	$1.1286e-02$	1.33	$7.8218e-03$	1.56	$1.3595e+01$	1.26	$7.3387e+00$	1.50
2	$4.0126e-03$	1.49	$2.4598e-03$	1.66	$5.1216e+00$	1.40	$2.3484e+00$	1.64
3	$1.4272e-03$	1.49	$8.1302e-04$	1.59	$1.8807e+00$	1.44	$7.5647e-01$	1.63
4	$5.0776e-04$	1.49	$2.7859e-04$	1.54	$6.8048e-01$	1.46	$2.4982e-01$	1.59
5	$1.8027e-04$	1.49	$9.7129e-05$	1.52	$2.4393e-01$	1.48	$8.4493e-02$	1.56
6	$6.3891e-05$	1.49	$3.4122e-05$	1.50	$8.6940e-02$	1.48	$2.9081e-02$	1.53
		1.50		1.50		1.50		1.50

shown in Tables 4.1 and 4.2. In the last row of each table, the theoretical convergence orders of the discretization errors are given.

TABLE 4.3
Relative $L^2(\Omega)$-, relative $H^1(\Omega)$-error of u_h, discrete $H^{\frac{1}{2}}(\gamma)$-error of the jump of u_h, discrete $H^{-\frac{1}{2}}(\gamma)$-error of the Lagrange multiplier and the convergence orders for the mortar method for linear finite elements.

l	$\|u - u_h\|_{0,\Omega}$		$\|u - u_h\|_{1,\Omega}$		$\|[u_h]\|_{\frac{1}{2},h,\gamma}$		$\|\lambda - \lambda_h\|_{-\frac{1}{2},h,\gamma}$	
0	$3.4682e-01$	–	$6.7315e-01$	–	$8.9691e-05$	–	$2.3970e+01$	–
1	$7.4666e-02$	2.21	$3.2348e-01$	1.05	$5.9368e-03$	–	$5.7759e+00$	2.02
2	$1.8362e-02$	2.02	$1.6083e-01$	1.00	$2.3203e-03$	1.35	$1.8070e+00$	1.68
3	$4.5632e-03$	2.00	$8.0237e-02$	1.00	$8.3504e-04$	1.47	$6.1755e-01$	1.55
4	$1.1380e-03$	2.00	$4.0075e-02$	1.00	$2.2307e-04$	1.90	$2.1577e-01$	1.52
5	$2.8419e-04$	2.00	$2.0027e-02$	1.00	$7.3692e-05$	1.59	$7.5913e-02$	1.51
6	$7.1004e-05$	2.00	$1.0011e-02$	1.00	$2.2804e-05$	1.69	$2.6779e-02$	1.50
		2.00		1.00		1.50		1.50

The discretization errors for the mortar method with linear finite elements, i.e., $p = 1$, are shown in Table 4.3. For the flux, we get the order $h^{\frac{3}{2}}$, although (2.7) gives us order one. But under the assumption that the energy error is equilibrated distributed, we can also show order $h^{\frac{3}{2}}$, see Remark 2.1. Comparing the discretization errors for both methods, the same qualitative and quantitative results can be observed for the L^2-norm and the H^1-norm. The numerical results confirm the predicted theoretical ones. For the weighted L^2-norm of the jump on the interface, we obtain in the mortar setting better results. The jump of the solution is smaller than in the case of the Nitsche formulation, see Tables 4.1 and 4.3. For the flux on the slave side, we find almost the same quantitative results. We note that the mesh on the slave side is finer than on the master side. As a consequence, we find in the Nitsche formulation that the error in the flux on the slave side is better than on the master side, see Table 4.2.

4.2. Influence of the Nitsche parameter θ. In a second test, we consider the influence of the stabilization parameter θ on the Nitsche method. We compare the discretization errors in the L^2-norm, the H^1-norm and the weighted jump for different parameters θ. On level 2, the influence on the L^2-error is presented in Figure 4.2, on the H^1-error in Figure 4.3, and on the jump on the interface in Figure 4.4. Increasing the Nitsche parameter θ results in smaller errors for the jump of the trace. The constant θ can be interpreted as a penalty factor. Thus, the bigger the stabilization parameter is, the higher is the penalization of a jump in the trace. As a consequence, the weighted L^2-norm of the jump in the trace decreases as θ increases. On the other hand, the continuity constant of the mesh dependent bilinear from increases as θ increases. Thus, the L^2- and H^1-errors increase, if θ tends to infinity. The influence on the L^2-norm is stronger than on the H^1-norm. In all cases, good numerical results can be only obtained if the stabilization parameter is bigger than a given limit. We observe a sharp bound for the parameter θ. If θ is smaller than this bound, the coercivity of the mesh dependent bilinear form is lost.

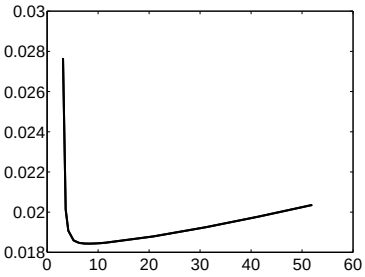

FIG. 4.2. $\|u - u_h\|_{0,\Omega}$ *versus* θ

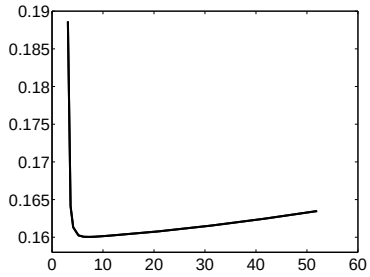

FIG. 4.3. $\|u - u_h\|_{1,\Omega}$ *versus* θ

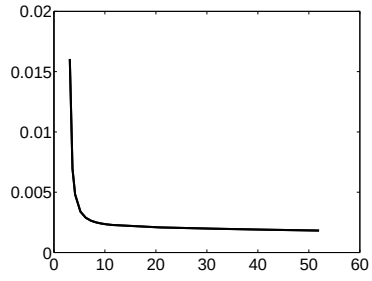

FIG. 4.4. $\|[u_h]\|_{\frac{1}{2},h,\gamma}$ *versus* θ

4.3. Quadratic finite elements. To give a numerical example for quadratic finite elements, we present the discretization errors for the Nitsche and the mortar method for the same example.

TABLE 4.4
Relative $L^2(\Omega)$-, relative $H^1(\Omega)$-error of u_h, discrete $H^{\frac{1}{2}}(\gamma)$-error of the jump of u_h and the convergence orders for the Nitsche method for quadratic finite elements.

level	$\|u - u_h\|_{0,\Omega}$		$\|u - u_h\|_{1,\Omega}$		$\|[u_h]\|_{\frac{1}{2},h,\gamma}$	
0	$3.500443e-02$	–	$1.374870e-01$	–	$4.466369e-03$	–
1	$4.356586e-03$	3.00	$3.394598e-02$	2.01	$8.326474e-04$	2.42
2	$5.213736e-04$	3.06	$8.354069e-03$	2.02	$1.512516e-04$	2.46
3	$6.290017e-05$	3.05	$2.065453e-03$	2.01	$2.708922e-05$	2.48
4	$7.692445e-06$	3.03	$5.130593e-04$	2.00	$4.819506e-06$	2.49
5	$9.499893e-07$	3.01	$1.278250e-04$	2.00	$8.546847e-07$	2.49
theory		3.00		2.00		2.50

TABLE 4.5
Discrete $H^{\frac{1}{2}}(\gamma)$-, discrete $H^{-\frac{1}{2}}(\gamma)$-error of u_h on the master and the slave side and the convergence orders for the Nitsche method for quadratic finite elements.

l	$\|u^1 - u_h^1\|_{\frac{1}{2},h,\gamma_1}$		$\|u^2 - u_h^2\|_{\frac{1}{2},h,\gamma_2}$		$\|(\boldsymbol{\sigma}^1 - \boldsymbol{\sigma}_h^1)n\|_{-\frac{1}{2},h,\gamma_1}$		$\|(\boldsymbol{\sigma}^2 - \boldsymbol{\sigma}_h^2)n\|_{-\frac{1}{2},h,\gamma_2}$	
0	$3.6599e-03$	–	$1.9184e-03$	–	$1.0782e+01$	–	$6.1068e+00$	–
1	$6.6100e-04$	2.46	$3.6049e-04$	2.41	$2.0037e+00$	2.42	$1.1559e+00$	2.40
2	$1.1792e-04$	2.48	$6.5837e-05$	2.45	$3.6345e-01$	2.46	$2.1152e-01$	2.45
3	$2.0939e-05$	2.49	$1.1819e-05$	2.47	$6.5046e-02$	2.48	$3.8006e-02$	2.47
4	$3.7098e-06$	2.49	$2.1050e-06$	2.48	$1.1568e-02$	2.49	$6.7722e-03$	2.48
5	$6.5654e-07$	2.49	$3.7351e-07$	2.49	$2.0511e-03$	2.49	$1.2018e-03$	2.49
		2.50		2.50		2.50		2.50

In Tables 4.4, 4.5 and 4.6, the discretization errors and the numerical convergence orders for quadratic finite elements are given. As in the linear case, our numerical results confirm the theoretical ones, and we observe the predicted convergence rates of orders h^2, h^3 and $h^{\frac{5}{2}}$ for the L^2-, H^1-norm and the weighted norms on the interface, respectively.

Asymptotically, we obtain for both methods almost the same quantitative results in the L^2- and the H^1-norm. As before, the weighted norm of the jump of the trace is smaller in the mortar setting than in the Nitsche formulation. This is also true for the error in the flux on the interface. The Lagrange multiplier of the mortar method yields better results than the flux computed directly from the discrete Nitsche solution. A small difference in the asymptotic convergence rates can be observed.

4.4. An Example with more than two subdomains. To show the flexibility of the methods, we consider an example with more than two subdomains. Let Ω be the domain given by $\Omega := \big[(0,1) \times (0,1)\big] \setminus \big[(0.25, 0.75) \times (0.25, 0.75)\big]$. This domain is decomposed into eight non

TABLE 4.6
Relative $L^2(\Omega)$-, relative $H^1(\Omega)$-error of u_h, weighted L^2-error of the jump of u_h, and the flux and the convergence orders for the mortar method for quadratic finite elements.

l	$\|u-u_h\|_{0,\Omega}$		$\|u-u_h\|_{1,\Omega}$		$\|[u_h]\|_{\frac{1}{2},h,\gamma}$		$\|\lambda-\lambda_h\|_{-\frac{1}{2},h,\gamma}$	
0	$4.2375e-02$	–	$1.4726e-01$	–	$1.7834e-03$	–	$5.9502e+00$	–
1	$4.9359e-03$	3.10	$3.4839e-02$	2.07	$3.1516e-04$	2.50	$8.4688e-01$	2.81
2	$5.6228e-04$	3.13	$8.4415e-03$	2.05	$5.5712e-05$	2.50	$1.2851e-01$	2.72
3	$6.5662e-05$	3.10	$2.0748e-03$	2.02	$9.8488e-06$	2.50	$2.0594e-02$	2.64
4	$7.8729e-06$	3.06	$5.1413e-04$	2.01	$1.5104e-06$	2.70	$3.4375e-03$	2.58
5	$9.6154e-07$	3.03	$1.2795e-04$	2.01	$1.8880e-07$	3.00	$5.8890e-04$	2.55
		3.00		2.00		2.50		2.50

overlapping subdomains, see Figure 4.5. At the bottom boundary segment, where $x_2 = 0$ holds, we impose homogeneous Dirichlet boundary conditions. At the top boundary segment, where $x_2 = 1$ holds, we have in the second component u_2 inhomogeneous Dirichlet data $u_2(x) = -0.1$ and in the first component u_1 homogeneous Neumann data. On any other boundary segment, homogeneous Neumann boundary conditions are imposed. The components of the stress tensor $\boldsymbol{\sigma}(u)$ obtained by the Nitsche method are presented in Figures 4.6-4.8. In the mortar setting, we obtain almost the same quantitative results.

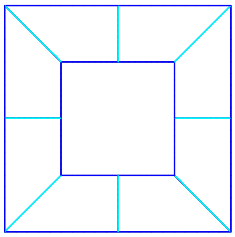

FIG. 4.5. *Domain* Ω

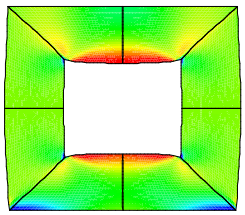

FIG. 4.6. $\boldsymbol{\sigma}_{11}$

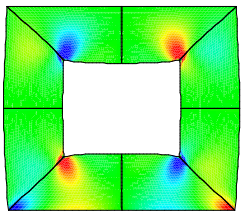

FIG. 4.7. $\boldsymbol{\sigma}_{12} = \boldsymbol{\sigma}_{21}$

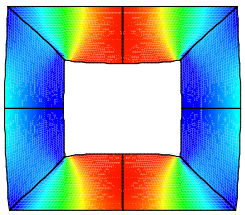

FIG. 4.8. $\boldsymbol{\sigma}_{22}$

4.5. Coupling of linear and quadratic finite elements. Now we will present an example, where different finite element orders are used in the subdomains. We consider the non convex domain $\Omega := \big[(-1,1)\times(-1,1)\big] \setminus \big[(0,1)\times(-1,0)\big]$ and define $\Omega_1 := \big\{(x_1,x_2)^\top \in \Omega : \max(|x_1|,|x_2|) < 0.25\big\}$ and $\Omega_2 := \Omega\backslash\overline{\Omega}_1$. Let $r := \|x\|_2$ and $\varphi := \operatorname{atan}(x_2/x_1)$ be the corresponding polar coordinates of $(x_1,x_2)^\top \in \mathbb{R}^2$. For each $\alpha \in \mathbb{R}$, we find that

$$u(r,\varphi) = r^\alpha \begin{pmatrix} 4\sin(\alpha\varphi) - \frac{\lambda+\mu}{\lambda+2\mu}\big(2\sin(\alpha\varphi) - \alpha\sin\big((2-\alpha)\varphi\big)\big) \\ -\frac{\lambda+\mu}{\lambda+2\mu}\alpha\cos\big((2-\alpha)\varphi\big) \end{pmatrix} \tag{4.1}$$

is a solution of $-\operatorname{div}\boldsymbol{\sigma}(u) = 0$ and $u \in \big[H^{1+\alpha-\varepsilon}(\Omega)\big]^2$, $\varepsilon > 0$. The singularity is at the corner $(0,0)^\top$ of the domain Ω. Due to this, we use a fine mesh and linear finite elements in Ω_1 and a coarse mesh and quadratic finite elements in Ω_2, see Figure 2.2. We restrict ourselves to the Nitsche method, but mortar techniques can be used as well. The numerical results are presented in Tables 4.7 and 4.8.

We set $\alpha = 2/3$ in (4.1) and find $u \in \big[H^{\frac{5}{3}-\varepsilon}(\Omega)\big]^2$, $\varepsilon > 0$. Although the solution has a singularity at $(0,0)^\top$, it is H^3-regular in the neighborhood of the interface. The convergence rates in the L^2-norm, the H^1-norm and for the jump of the trace are given in Table 4.7. Due to the singularity, we cannot expect high order convergence rates. Our numerical results show asymptotically a convergence order of $h^{\frac{4}{3}}$ for the L^2-error and of order $h^{\frac{2}{3}}$ for the H^1-error. Although, we use linear finite elements on Ω_1 and quadratic finite elements on Ω_2, the convergence rates on the interface for the trace are asymptotically almost the same, see Table 4.8. In the case of the error for the flux, the situation is different. We observe better convergence rates for the

quadratic finite element solution on Ω_2. The convergence rates for the flux are close to the optimal ones in the case of full regularity. The results for the trace reflect in a more sensitive way the lower regularity than the ones for the flux.

TABLE 4.7
Relative $L^2(\Omega)$-, relative $H^1(\Omega)$-error of u_h, discrete $H^{\frac{1}{2}}(\gamma)$-error of the jump of u_h and the convergence orders for the Nitsche method for coupling of linear and quadratic finite elements in domain 2.2 under solution (4.1) using $\alpha = 2/3$.

level	$\|u-u_h\|_{0,\Omega}$		$\|u-u_h\|_{1,\Omega}$		$\|[u_h]\|_{\frac{1}{2},h,\gamma}$	
0	$5.377395e-03$	–	$2.041094e-01$	–	$1.542755e-02$	–
1	$9.611221e-04$	2.48	$2.945791e-02$	2.79	$2.533126e-03$	2.61
2	$3.069164e-04$	1.65	$1.801019e-02$	0.71	$4.928690e-04$	2.36
3	$1.201425e-04$	1.35	$1.136175e-02$	0.66	$1.402242e-04$	1.81
4	$4.859550e-05$	1.30	$7.187206e-03$	0.66	$6.087054e-05$	1.20
5	$1.979989e-05$	1.30	$4.541728e-03$	0.66	$2.532764e-05$	1.27

TABLE 4.8
Discrete $H^{\frac{1}{2}}(\gamma)$-, discrete $H^{-\frac{1}{2}}(\gamma)$-error of u_h on the master and the slave side and the convergence orders for the Nitsche method for coupling of linear and quadratic finite elements in domain 2.2 under solution (4.1) using $\alpha = 2/3$.

l	$\|u^1-u_h^1\|_{\frac{1}{2},h,\gamma_1}$		$\|u^2-u_h^2\|_{\frac{1}{2},h,\gamma_2}$		$\|(\boldsymbol{\sigma}^1-\boldsymbol{\sigma}_h^1)n\|_{-\frac{1}{2},h,\gamma_1}$		$\|(\boldsymbol{\sigma}^2-\boldsymbol{\sigma}_h^2)n\|_{-\frac{1}{2},h,\gamma_2}$	
0	$4.6504e-02$	–	$2.5441e-02$	–	$5.2971e+00$	–	$8.3329e+01$	–
1	$1.5402e-02$	1.59	$6.7803e-03$	1.90	$1.5616e+00$	1.76	$6.4605e+00$	3.69
2	$7.4463e-03$	1.05	$2.9718e-03$	1.19	$5.5855e-01$	1.48	$1.5345e+00$	2.07
3	$4.2627e-03$	0.80	$1.6715e-03$	0.83	$2.1670e-01$	1.36	$3.2015e-01$	2.26
4	$2.4889e-03$	0.77	$9.6221e-04$	0.80	$8.2547e-02$	1.39	$6.1775e-02$	2.37
5	$1.4569e-03$	0.77	$5.5619e-04$	0.79	$3.0499e-02$	1.44	$1.2107e-02$	2.35

4.6. Multigrid convergence rates. Finally, we present some multigrid convergence rates. Here, we restrict ourselves to the first example presented in Section 4.1 for linear finite elements. We use two different smoothers and compare the influence of the number of smoothing steps on both methods.

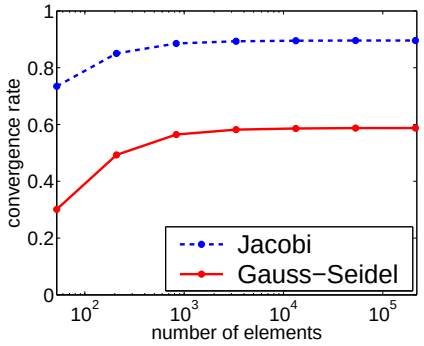

FIG. 4.9. *$\mathcal{W}(1,1)$-cycle for Nitsche*

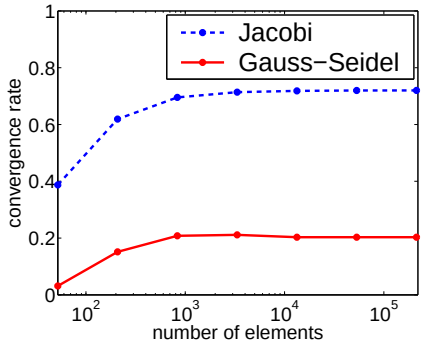

FIG. 4.10. *$\mathcal{W}(3,3)$-cycle for Nitsche*

The asymptotic convergence rates for the Nitsche method for the $\mathcal{W}$-cycle with one and three pre- and post-smoothing steps are given in Figures 4.9 and 4.10. Figures 4.11 and 4.12 show the asymptotic convergence rates for the mortar method. We observe in the case of a symmetric Gauß–Seidel smoother better convergence rates for the Nitsche method than for the mortar method. However, using a damped Jacobi smoother with damping factor 0.8, the convergence rates are the same. In all cases, we obtain level independent convergence rates as predicted by the theory. Level

independent results can be also observed for the $\mathcal{V}$-cycle and one smoothing step in the mortar method, see [WK01]. This is not the case for the Nitsche formulation. To obtain level independent convergence rates for the $\mathcal{V}$-cycle in the mortar setting, we use a modified transfer operator. This operator exploits that $Q_h^l u_h^l = 0$ for all refinement levels l, i.e., the jump of the trace is orthogonal on the Lagrange multiplier space. Here Q_h^l is the projection operator on level l defined by (2.20). In the Nitsche formulation such orthogonality does not hold. Thus, it is not clear how to construct a modified transfer operator for the Nitsche method yielding optimal $\mathcal{V}$-cycle results. The Lagrange multiplier space of the mortar methods guarantees level independent $\mathcal{V}$-cycle results whereas in the Nitsche method no level independent convergence rates for the $\mathcal{V}$-cycle can be observed.

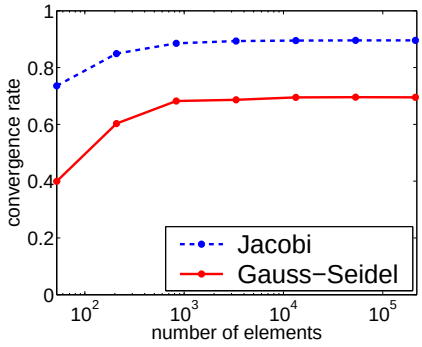

FIG. 4.11. $\mathcal{W}(1,1)$-*cycle for mortar*

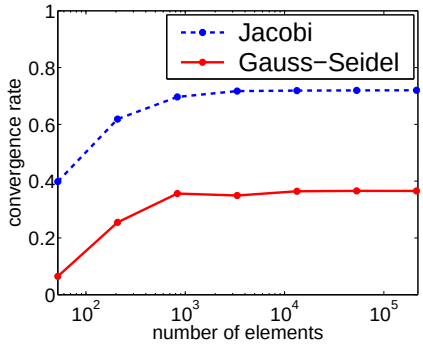

FIG. 4.12. $\mathcal{W}(3,3)$-*cycle for mortar*

REFERENCES

[BBJ+97] P. Bastian, K. Birken, K. Johannsen, S. Lang, N. Neuß, H. Rentz–Reichert, and C. Wieners. UG – a flexible software toolbox for solving partial differential equations. *Computing and Visualization in Science*, 1:27–40, 1997.

[BD98] D. Braess and W. Dahmen. Stability estimates of the mortar finite element method for 3–dimensional problems. *East–West J. Numer. Math.*, 6:249–263, 1998.

[Ben99] F. Ben Belgacem. The mortar finite element method with Lagrange multipliers. *Numer. Math.*, 84(2):173–197, 1999.

[BF91] F. Brezzi and M. Fortin. *Mixed and hybrid finite element methods.* Springer–Verlag, New York, 1991.

[BH99] R. Becker and P. Hansbo. A finite element method for domain decompositions with non–matching grids. *Preprint, INRIA, Sophia Antipolis*, 3613, January 1999.

[BHS01] R. Becker, P. Hansbo, and R. Stenberg. A finite element method for domain decomposition with non–matching grids. Technical Report 15, Chalmers University of Technology, 2001. to appear in M2AN.

[BM97] F. Ben Belgacem and Y. Maday. The mortar element method for three dimensional finite elements. *M2AN*, 31:289–302, 1997.

[BMP93] C. Bernardi, Y. Maday, and A.T. Patera. Domain decomposition by the mortar element method. In H. Kaper et al., editor, *Asymptotic and numerical methods for partial differential equations with critical parameters*, pages 269–286. Reidel, Dordrecht, 1993.

[BMP94] C. Bernardi, Y. Maday, and T. Patera. A new confirming approach to domain decomposition: The mortar element method. In *Nonlinear Partial Differential Equations and Their Applications.* Pitman, 1994.

[Bra95] J.H. Bramble. *Multigrid Methods.* Longman Scientific & Technical, 1995.

[DL88] R. Dautray and J.L. Lions. *Mathematical Analysis and Numerical Methods for Science and Technology*, volume 8. Springer, 1988.

[Hac85] W. Hackbusch. *Multi-Grid Methods and Applications.* Springer, 1985.

[HN01] B. Heinrich and S. Nicaise. Nitsche mortar finite element method for transmission problems with singularities. *Preprint-Reihe des Chemnitzer SFB 393*, 1, 2001.

[HP00] B. Heinrich and K. Pietsch. Nitsche type mortaring for some elliptic problem with corner singularities. *Preprint-Reihe des Chemnitzer SFB 393*, 34, 2000.

[Nit71] J. Nitsche. Über ein Variationsprinzip zur Lösung von Dirichlet-Problemen bei Verwendung von Teilräumen, die keinen Randbedingungen unterworfen sind. *Abhandlungen aus den Mathematischen Seminaren der Universität Hamburg*, 36, 1970/71.

[Tho97] V. Thomée. *Galerkin Finite Element Methods for Parabolic Problems.* Springer, 1997.

[Vas01] C. Kim; R.D. Lazarov; J.E. Pasciak; P.S. Vassilevski. Multiplier spaces for the mortar finite element method in three dimensions. *SIAM J. Numer. Anal.*, 39(2):519–538, 2001.

[WK01] B.I. Wohlmuth and R.H. Krause. Multigrid methods based on the unconstrained product space for mortar finite element discretizations. *SIAM J. Numer. Anal.*, 39:192–213, 2001.

[Woh00] B.I. Wohlmuth. A mortar finite element method using dual spaces for the Lagrange multiplier. *SIAM J. Numer. Anal.*, 38:989–1012, 2000.

[Woh01] B.I. Wohlmuth. *Discretization Methods and Iterative Solvers Based on Domain Decomposition*. Springer, 2001.

Achim Fritz
Pfaffenwaldring 57
70569 Stuttgart
Germany

Stefan Hüeber
Pfaffenwaldring 57
70569 Stuttgart
Germany
E-Mail: hueeber@ians.uni-stuttgart.de
WWW: http://www.ians.uni-stuttgart.de/nmh/hueeber/hueeber.shtml

Barbara I. Wohlmuth
Pfaffenwaldring 57
70569 Stuttgart
Germany
E-Mail: wohlmuth@ians.uni-stuttgart.de
WWW: http://www.ians.uni-stuttgart.de/nmh/wohlmuth/wohlmuth.shtml

Erschienene Preprints ab Nummer 2003/001

Komplette Liste: `http://preprints.ians.uni-stuttgart.de`

2003/001 *Lamichhane, B. P., Wohlmuth, B. I.*: Mortar Finite Elements for Interface Problems.

2003/002 *Dryja, M., Gantner, A., Widlund, O. B., Wohlmuth, B. I.*: Multilevel Additive Schwarz Preconditioner For Nonconforming Mortar Finite Element Methods.

2003/003 *Klimke, A., Hanss, M.*: On the Reliability of the In¤uence Measure in the Transformation Method of Fuzzy Arithmetic.

2003/004 *Klimke, A.*: RANDEXPR: A Random Symbolic Expression Generator.

2003/005 *Klimke, A.*: How to Access Matlab from Java.

2003/006 *Merkle, T.*: Phase separation in solid mixtures under elastic loadings with application to solder materials.

2003/007 *Lamichhane, B. P., Wohlmuth, B. I.*: Second Order Lagrange Multiplier Spaces for Mortar Finite Elements in 3D.

2003/008 *Fritz, A., Hüeber, S., Wohlmuth, B. I.*: A comparison of mortar and Nitsche techniques for linear elasticity.